Strain engineering in AlGaN/GaN HEMTs for performance enhancement

E. Mohapatra and R.K. Nanda

Department of Electronics and Communication Engineering,
Siksha 'O' Anusandhan (Deemed to be University),
Bhubaneswar, Odisha, 751030, India
Email: eleenamohapatra@soa.ac.in
Email: rajibnanda@soa.ac.in

S. Das

Department of Electronics and Communication Engineering,
Silicon Institute of Technology,
Bhubaneswar, Odisha, 751024, India
Email: sanghamitra.das@silicon.ac.in

T.P. Dash*, J. Jena, S. Dey and C.K. Maiti

Department of Electronics and Communication Engineering,
Siksha 'O' Anusandhan (Deemed to be University),
Bhubaneswar, Odisha, 751030, India
Email: taradash@soa.ac.in
Email: jhansiranijena@soa.ac.in
Email: supravadey@soa.ac.in
Email: ckmaiti@soa.ac.in
*Corresponding author

Abstract: In the first part of this work, using TCAD simulations, we examine the breakdown voltage as a function of field plate geometry. In the second part, we show that field plate-based GaN HEMT structures can be optimised to have effectively reduced undesirable parasitic capacitances to greatly improve both the high transconductance and current gain cut-off frequency simultaneously. We report a new generation of high performance AlGaN/GaN HEMTs grown on high resistivity SiC substrates. We examine the small signal and large signal device performances against technological parameters such as the gate length, field plate length, and the source-drain contact separation. The device with a gate length of 0.25 μm and field plate length of 0.3 μm exhibits a maximum dc drain current density of 3.66 A/mm at VGS = 3 V with an extrinsic transconductance of 233.6 mS/mm and an extrinsic current gain cut-off frequency (f_t) of 78.9 GHz.

Keywords: HEMT; AlGaN/GaN; SiC; field plate; drift-diffusion model; hydrodynamic model; TCAD.

Reference to this paper should be made as follows: Mohapatra, E., Nanda, R.K., Das, S., Dash, T.P., Jena, J., Dey, S. and Maiti, C.K. (2020) 'Strain engineering in AlGaN/GaN HEMTs for performance enhancement', *Int. J. Nano and Biomaterials*, Vol. 9, Nos. 1/2, pp.34–49.

Copyright © 2020 Inderscience Enterprises Ltd.

Biographical notes: E. Mohapatra received his MTech in VLSI and Embedded System Design from Biju Patnaik University of Technology, India in 2011. She is currently pursuing her PhD at Sikhsha 'O' Anusandhan (Deemed to be University). Her current research interests include nanoelectronic devices, FinFETs, and gate-all-around nanodevices.

R.K. Nanda received his BTech degree in Electronics and Telecommunication Engineering from University College of Engineering, Burla, India in 2008 and MTech degree in Electronics and Communication Engineering from IIT Kharagpur, India in 2015. He is currently working as an Assistant Professor at Sikhsha 'O' Anusandhan (Deemed to be) University, Bhubaneswar, India. His research interest lies in device modelling and simulation.

S. Das received her Master's degree in Technology in VLSI Design Engineering in 2012 and Bachelor's degree in Technology in Electronics and Telecommunication Engineering in 2009 form Biju Patnaik University of Technology (BPUT), India. She is currently pursuing her PhD as a full-time Research Scholar in Sikhsha 'O' Anusandhan University, India. Her research focus is mostly on reliability analysis of band engineered devices.

T.P. Dash received his Bachelor's degree in Technology in Electronics and Telecommunication Engineering from Biju Patnaik University of Technology, India in 2009 and Master's degree in Electronics Communication Engineering from Indian Institute of Technology Kharagpur, Kharagpur, India in 2012. He is currently working as an Assistant Professor at Sikhsha 'O' Anusandhan (Deemed to be University) and is pursuing his PhD in Heterojunction Devices. His research interests include performance analysis of 2D and 3D devices using TCAD tools.

J. Jena received her MTech in Electronics Communication Engineering from Siksha 'O' Anusandhan University, Bhubaneswar, Odisha, India in 2013. She is currently working as an Assistant Professor at Sikhsha 'O' Anusandhan (Deemed to be University). Her research interests include FinFETs and nanoelectronic devices.

S. Dey received his Bachelor's degree in Technology in Electronics and Telecommunication Engineering from Biju Patnaik University of Technology, Rourkela, Odisha, India in 2011 and Master's degree in VLSI Signal Processing from Veer Surendra Sai University of Technology Burla, Sambalpur, Odisha, India in 2016. She is currently pursuing her PhD in Sikhsha 'O' Anusandhan (Deemed to be University) in advanced MOSFET devices.

C.K. Maiti had been with the IIT-Kharagpur since 1976 till 2014 in various academic positions and was head of the department (2009–2012). He was a Visiting Professor at Queen's University, Belfast, UK from 2004 to 2006. He received INSA-Royal Society (UK) Exchange of Scientists Fellowship in 2003. He is a life senior member of the IEEE, USA. He is interested in semiconductor device/process simulation research using TCAD and microelectronics education.

This paper is a revised and expanded version of a paper entitled 'High frequency performance of AlGaN/GaN HEMTs fabricated on SiC substrates' presented at DevIC-2019, IEEE KGEC, West Bengal, 23–24 March 2019.

1 Introduction

Power devices are gaining more popularity nowadays with the extensive use of electronic devices in every field as these have a major influence on the system cost and efficiency. Importance of TCAD tools is also well known for the device early-stage design to perform performance evaluation by using computer-based models to compensate for the expensive prototyping and large signal experimental characterisation of the millimetre and sub-millimetre wave devices. Combination of both the high transconductance and current gain cut-off frequency (f_t) is desirable for power semiconductor devices which is a major part of the power electronic systems.

GaN/SiC technology is preferred for industrial use as the SiC substrates are more cost effective. The GaN/SiC HEMT technology can completely replace the presently used substrate/GaN epi-wafer technology due to high thermal conductivity (+30%) of the semi-insulating SiC substrate along with its low cost. GaN has a hexagonal structure named "wurtzite" and has a bandgap energy of 3.4 eV. The energy bandgap, breakdown field and electron mobility in GaN are very high which makes it extremely suitable to be used in power electronic applications (Mishra et al., 2002). The switching frequencies of GaN HEMTs can be very high in the range of GHz and the device shows high power conversion efficiency (Wu et al., 2008).

Device performance can be improved even without any change in the semiconductor material properties, however, with dedicated new device structures and fabrication methods. For example, for GaN-based HEMTs, among one of the techniques to improve performance is the introduction of field plate (FP) in the device (Karmalkar and Mishra, 2001). The role of a FP is to modify the electric field profile and to decrease its peak value on the drain side of the gate edge, hence reducing high-field trapping effects and increasing breakdown voltage. The FP technique has resulted in 2-to-4 times performance enhancement in RF GaN-based devices. Currently, FP technique is the most widely used approach and even employed in the commercial of AlGaN/GaN HEMTs for electric field (E-field) modulation and breakdown voltage improvements (Ando et al., 2003). The FP and its extension are favourable to decrease the electric field intensity at the gate edge and hence reduces the electron trapping probability which results in the reduction of low frequency noise (Chiu et al., 2013). Due to the piezoelectric nature of GaN, the 2D electron gas (2DEG) in AlGaN/GaN HEMT can also be engineered by strain. Strain distributions within nanoscale non-planar device structures can be expected to behave differently compared to that of a planar structure due to the nature of the 3D device architecture. Because the modulation of strain becomes more pronounced with device scaling, the influence of the variation in strain on the device characteristics is of great concern. Therefore, as the geometries of these 3D device structures become more complex, it is important to understand how strain develops within the nanoscale device structure. To investigate the FP length dependence of the induced stress underneath the gate region, the stress distributions have been simulated using TCAD simulation tool (*Victory Device User Manual*, 2017).

In this paper, we have the five Sections including the introduction part as Section 1. The design aspects of FP-based GaN HEMTs are presented in Section 2. The device structure detail and stress simulation basics and FP geometry dependent stress profiles are presented. Section 3 includes the high frequency HEMTs design aspects. The device structure detail and simulation environment are discussed in this Section. The results and discussion of the high frequency simulation are presented in Section 4 where the device

characteristics are presented. The effects of dimensions of FP on the small signal gain and cut-off frequency are also presented in this Section. Conclusions drawn from this study are presented in Section 5.

2 Stress-engineered GaN-HEMTs design

Strain distributions within nanoscale non-planar device structures can be expected to behave differently compared to that of a planar structure due to the nature of the 3D device architecture. Because the modulation of strain becomes more pronounced with device scaling, the influence of the variation in strain on the device characteristics is of great concern. Therefore, as the geometries of these 3D device structures become more complex, it is important to understand how strain develops within the nanoscale HEMT device structures. The device under consideration consists of a simple 0.4 μm gate length GaN HEMT augmented with a FP used to increase the breakdown voltage (Karmalkar and Mishra, 2001). The role of a FP is to modify the electric field profile and to decrease its peak value on the drain side of the gate edge, hence reducing high-field trapping effects and increasing breakdown voltage. To examine the relationship between FP geometry and breakdown voltage, both the FP length and thickness were changed. The gate electrode in HEMT structures is a Schottky contact. To improve convergence, especially in wide bandgap materials, the thermal generation was provided by SRH model. In order to simulate the avalanche breakdown, the Selberherr impact ionisation model is used. All the models used in this study, including the quantum models, were calibrated with previously reported results (Karmalkar and Mishra, 2001). The detailed GaN material parameters considered in simulation has been listed in Table 1. The model and material parameters have also been incorporated in 2D device simulator ATLAS (*ATLAS Users Manual*, 2017).

Table 1 GaN material parameters used in simulation

Parameter	*GaN*	*Units*
Band gap	3.43	eV
Lattice constant	3.189	A
Critical elec. field (Ec)	3.75	MV/cm
Hole life time(auger)	1×10^{-9}	s
Electron life time (auger)	1×10^{-9}	s
Peak velocity	2.2×10^{7}	cm/s
Saturation velocity	1.125×10^{7}	cm/s
Hole mobility	10	cm^2/Vs
Electron mobility	525	cm^2/Vs
Donor energy level	0.016	eV
Acceptor energy level	0.175	eV

We have quantitatively characterised the evolution of the stress profile due to the presence of FP as a function of its geometry and confirm that they obey elastic deformation based on the model that depends on the relative difference between the equilibrium GaN and AlGaN lattice constants. In the AlGaN/GaN heterostructure, the

2-DEG is induced by the piezoelectric charge effect without doping. The polarisation of GaN crystal is able to change under external stress or strain along the c-axis due to the non-ideality of the equilibrium lattice parameters. These parameters will change to accommodate the stress. The generation of an electric polarisation field in a crystal, which is under strain is called piezoelectric polarisation.

Nitride-based materials (GaN and AlGaN) are characterised by spontaneous polarisation. So, the mismatch at the interface between AlGaN and GaN induces stress which results in a piezoelectric polarisation. These properties lead to the appearance of fixed charges at the interface and surface of materials (Ambacher et al., 2000). At the microscopic level, a strain parallel or perpendicular to the c-axis induces an internal displacement of the metal sublattice with respect to the nitrogen ones. In a pseudomorphic wurtzite hetero-epitaxial growth process, the crystal deformation (strain) of the epilayer can be related to the stress. The out of plane lattice parameter (c-parameter) of the epilayer changes depending on the in plane strain induced during the growth. The stress-strain relation and also the relationship between the out of plane lattice parameter (c-parameter) to that of in-plane lattice parameter (a-parameter) can be found from the Hooke's law:

$$\vec{\sigma} = C.\vec{\varepsilon} \tag{1}$$

where $\vec{\sigma}$, $\vec{\varepsilon}$ are stress and strain tensors and C is the elastic coefficient tensor. Using Voigt notation 17 for hexagonal crystal system, we can express them as follows:

$$\vec{\sigma} = \begin{bmatrix} \sigma_{xx} \\ \sigma_{yy} \\ \sigma_{zz} \\ \sigma_{yz} \\ \sigma_{zx} \\ \sigma_{xy} \end{bmatrix} \quad \vec{\varepsilon} = \begin{bmatrix} \varepsilon_{xx} \\ \varepsilon_{yy} \\ \varepsilon_{zz} \\ 2\varepsilon_{yz} \\ 2\varepsilon_{zx} \\ 2\varepsilon_{xy} \end{bmatrix} \quad C = \begin{bmatrix} C_{11} & C_{12} & C_{13} & 0 & 0 & 0 \\ C_{12} & C_{11} & C_{13} & 0 & 0 & 0 \\ C3 & C_{13} & C_{33} & 0 & 0 & 0 \\ 0 & 0 & 0 & C_{44} & 0 & 0 \\ 0 & 0 & 0 & 0 & C_{44} & 0 \\ 0 & 0 & 0 & 0 & 0 & \frac{C_{11} - C_{12}}{2} \end{bmatrix} \tag{2}$$

If we consider that the growth direction of an epilayer is along Z axis, then the stress in grown epilayer will take place along the two perpendicular directions of the in-plane axes (along X and Y axes). In such case, the heterostructure is known to be in a biaxial stress state. In general, the strain tensor components along different directions are expressed in terms of the lattice constants as:

$$\in_{xx} = \in_{yy} = \frac{a - a_0}{a_0}; \quad \in_{zz} = \frac{c - c_0}{c_0} \tag{3}$$

where a_0 and c_0 are relaxed epilayer's unit cell parameters and a and c are the strained epilayer's unit cell parameters.

$$\sigma = \left(c_{11} + c_{12} - \frac{2c_{13}^2}{c_{33}} \right) \varepsilon \tag{4}$$

where $\sigma = \sigma_{xx} = \sigma_{yy}$, and $\forall_i \neq j$, $\sigma_{ij} = 0$.

and $\varepsilon_{zz} = \frac{2c_{13}}{c_{33}}\varepsilon$ (5)

where $\varepsilon = \varepsilon_{xx} = \varepsilon_{yy}$.

Therefore, for the biaxial stress condition, equation (4) gives us the stress-strain relation of the epilayer and equation (5) correlates the extension or contraction along the growth direction ε_{zz} (Z-axis) of the epilayer to that of any lateral deformation ε. In uniaxial stress condition (i.e., $\sigma_{xx} \neq \sigma_{yy} = \sigma_{zz} = 0$), the correlation between ε_{xx} and ε_{zz} can be expressed from equations (1) and (2) as:

$$\varepsilon_{zz} = -\frac{c_{13}\left(c_{11} - c_{12}\right)}{c_{11}c_{33} - c_{13}^2}\varepsilon_{xx} \quad (6)$$

For a pseudomorphic heteroepitaxial growth process, from equations (5) and (6), we can express the deformed lattice parameter of any epilayer along the growth direction as:

$$c = c_0\left[1 - \frac{2c_{13}}{c_{33}}\left(\frac{a - a_0}{a_0}\right)\right] \quad (7)$$

for biaxial stress condition and

$$c = c_0\left[1 - \left\{\frac{c_{13}\left(c_{11} - c_{12}\right)}{c_{11}c_{33} - c_{13}^2}\right\}\left(\frac{a - a_0}{a_0}\right)\right] \quad (8)$$

for uniaxial stress condition.

The critical variables associated with the FP and the crucial semiconductor region beneath are readily seen to be: the three geometrical variables, namely the FP length, the insulator thickness and gate-drain separation, and the two material variables, namely the channel electron concentration over and the insulator dielectric constant.

In Figure 1 shows the schematic cross-section view of the GaN HEMT with a FP. To improve the off-state behaviour, a single field plated structure is considered and the FP is connected to the gate metal with a specific distance to the channel. The mechanical stress distribution due to the presence of the FP is shown;

a the Von Mises stress

b stress in the xx direction

c strain in the xx-direction.

Stress generated is found to be compressive in nature. The FP length dependence of the breakdown voltage is shown in Figure 2. As expected, the breakdown voltage increases as the FP length increases which however, affects the high frequency performance as will be discussed in Section 3. The field distribution due to the presence of a single FP is shown in Figure 3. It is observed that the peak field distribution occurs at the edge of the FP. The potential distribution beneath the FP is shown in Figure 4. The role of a FP is to modify the electric field profile and to decrease its peak value on the drain side of the gate edge, which is clearly visible from Figure 4.

Figure 1 Mechanical stress distribution in the FP, (a) Von Mises STRESS, (b) stress in xx-direction (c) strain in xx-direction (see online version for colours)

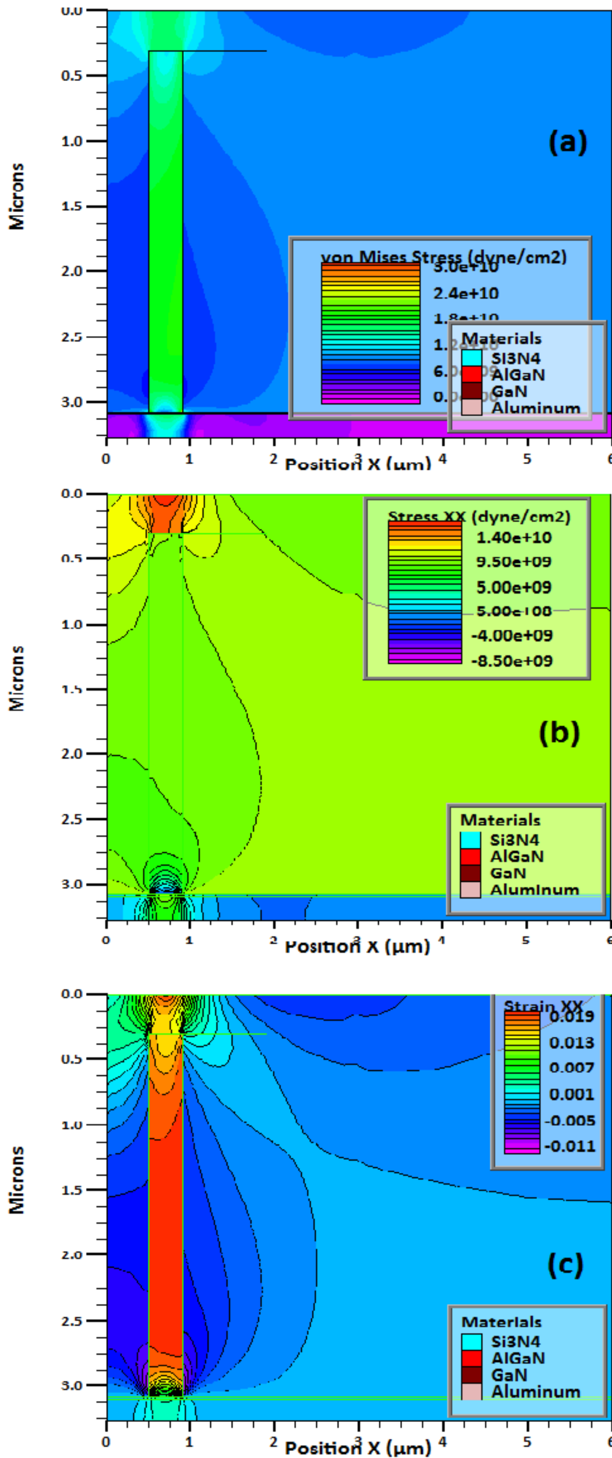

Figure 2 FP length vs. breakdown voltage characteristics (see online version for colours)

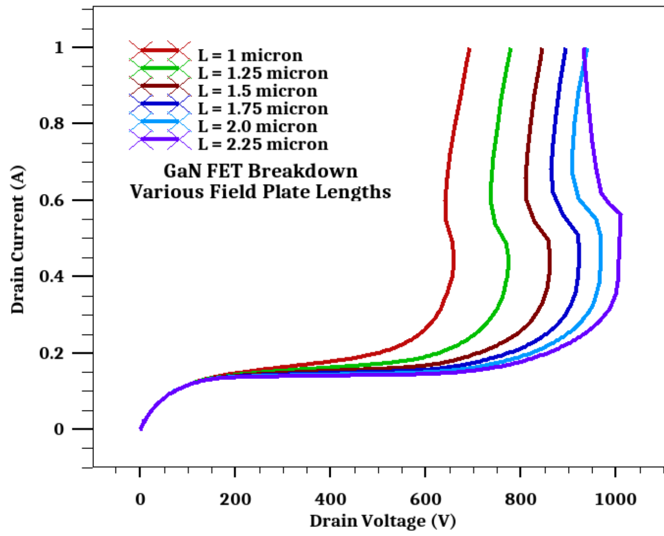

Figure 3 Electric field distribution at FP edge (see online version for colours)

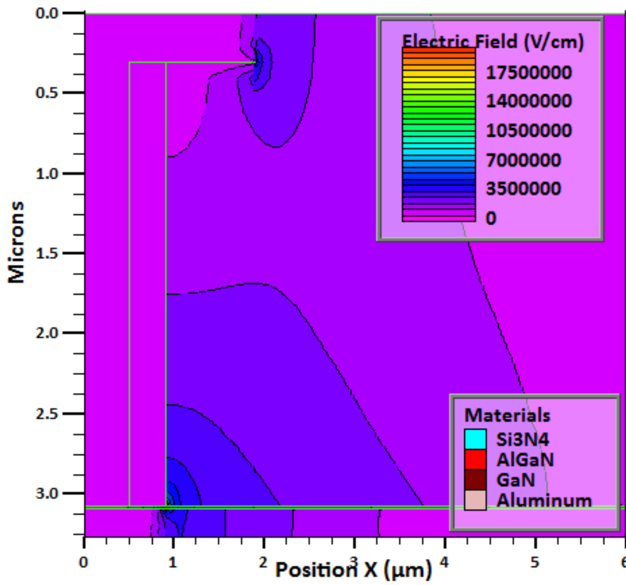

Figure 4 Potential distribution at the FP edge (see online version for colours)

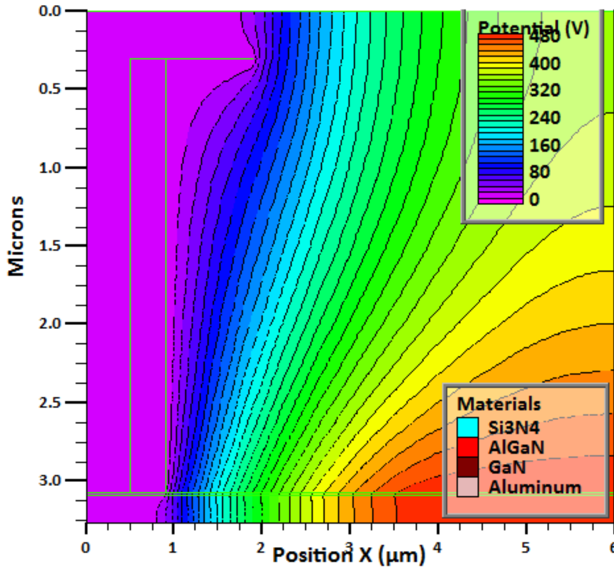

3 RF performance simulation

The device structures considered for high frequency (RF) simulation were epitaxially grown using MOCVD on SiC substrates. The heterostructure consists of a highly resistive c-plane GaN buffer, 50 nm thick AlGaN barrier over the GaN buffer and on the top a 5 nm thin GaN cap layer. Between the different layers of the HEMT, a sheet charge forms, that is assumed to be -4×10^{14} cm^{-2}, -2.5×10^{14} cm^{-2} and 9.4×10^{14} cm^{-2} for cap and spacer charge, barrier and cap charge and semiconductor and barrier charge, respectively. The 2DEG formed at the heterostructure interface resulted in a sheet carrier concentration of 9.4×10^{14} cm^{-2} and mobility of 1,600 cm^2/V.s. Ohmic contacts were formed after epitaxial growth. The nitride-assisted T-gate is defined by e-beam lithography with a gate length of 0.25 μm. The detailed technological parameters considered in simulation has been listed in Table 2. The schematic of AlGaN/GaN HEMT without and with FP are shown in Figures 5(a) and 5(b), respectively. The net doping concentrations in different regions of AlGaN/GaN HEMT is shown in Figure 5(c).

Here 2D simulations have been performed with the device simulation tool MINIMOS-NT (*Minimos-NT User Manual*, 2017) for the heterostructure device analysis with FPs (Vitanov et al., 2007). The transport models have been chosen in such a way that it should be computationally efficient with the highest precision. The hydrodynamic model has been implemented in this work due to the fact that the drift-diffusion (DD) model is not suitable in terms of accuracy for submicron GaN devices (Vitanov et al., 2012). The hole transport has been neglected because the AlGaN/GaN HEMTs are unipolar devices and a constant hole temperature of 300 K is maintained.

Table 2 Parameters for AlGaN/GaN HEMTs used in simulation

Parameters	*Value*
Gate length (L_g)	250 nm
FP length	0.3 μm
Cap and spacer charge	-4×10^{14} cm^{-2}
Barrier and cap charge	-2.5×10^{14} cm^{-2}
Semiconductor and barrier charge	9.4×10^{14} cm^{-2}
Barrier layer	50 nm
Cap layer	5 nm

Figure 5 Schematic of AlGaN/GaN HEMT (a) without FP, (b) with FP, and (c) AlGaN/GaN HEMT with net doping concentration (see online version for colours)

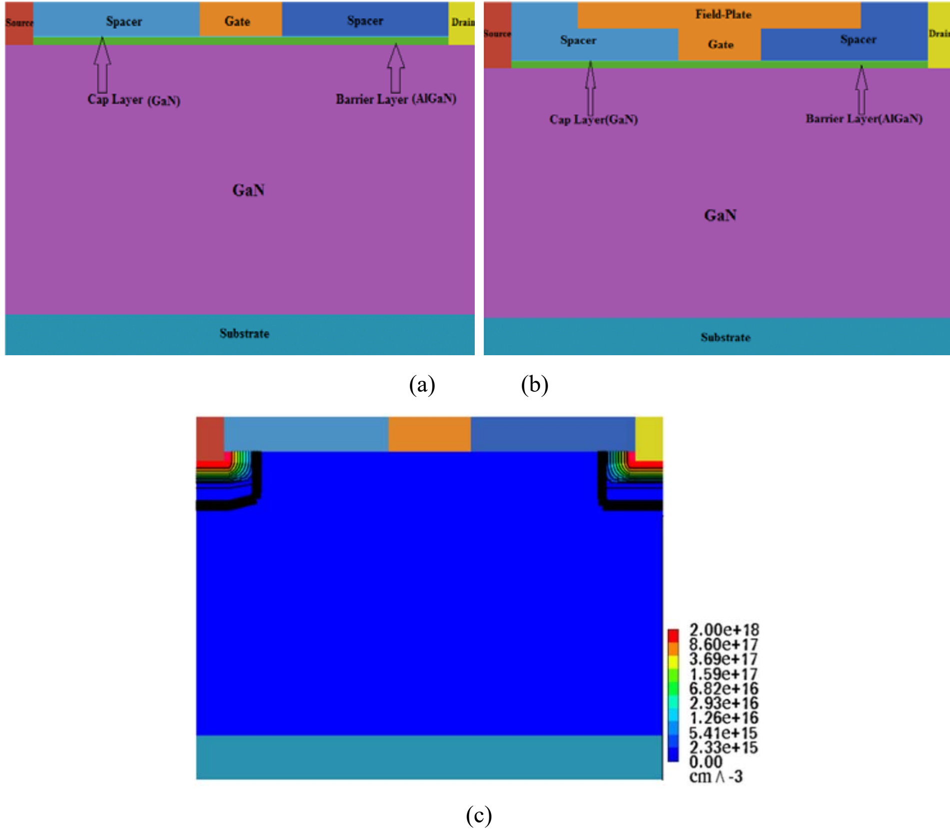

The basic semiconductor equations for the simulation of HEMT is given below. The electron and hole current densities are given by the expressions (Vitanov et al., 2012):

$$J_n = q \cdot \mu_n \cdot n \cdot \left(grad\left(\frac{\varepsilon_C}{q} - \psi \right) + \frac{k_B}{q} \cdot \frac{N_{C,0}}{n} \cdot rad\left(\frac{n \cdot T_L}{N_{C,0}} \right) \right) \tag{9}$$

$$J_p = q \cdot \mu_p \cdot p \cdot \left(grad\left(\frac{\varepsilon_V}{q} - \psi \right) + \frac{k_B}{q} \cdot \frac{N_{V,0}}{p} \cdot rad\left(\frac{p \cdot T_L}{N_{V,0}} \right) \right) \tag{10}$$

where J_n is the electron current density, J_p is the hole current density, μ_n and μ_p are the carrier mobilities, ε_C and ε_V are the position dependent band edge energies, $N_{C,0}$ and $N_{V,0}$ are the effective density of states, and T_L is the lattice temperature.

For the electron and hole mobilities, μ_n and μ_p respectively, the model considers a field dependence for the DD model and a carrier temperature dependence for the HD model. The energy transport equations for the HD model are given as:

$$div\ S_n = grad\left(\frac{\varepsilon_C}{q} - \psi \right) \cdot J_n - \frac{3 \cdot k_B}{2} \cdot \left(\frac{\partial (n \cdot T_n)}{\partial t} + R \cdot T_n + n \cdot \frac{T_n - T_L}{\tau_{\in,n}} \right) \tag{11}$$

$$div\ S_p = grad\left(\frac{\varepsilon_V}{q} - \psi \right) \cdot J_p - \frac{3 \cdot k_B}{2} \cdot \left(\frac{\partial (p \cdot T_p)}{\partial t} + R \cdot T_p + p \cdot \frac{T_p - T_L}{\tau_{\in,p}} \right) \tag{12}$$

where S_n and S_p are the energy fluxes, $\tau_{\in,n}$ and $\tau_{\in,p}$ are the energy relaxation times.

$$S_n = -k_n \cdot grad\ T_n - \frac{5}{2} \cdot \frac{k_B T_n}{q} \cdot J_n \tag{13}$$

where k_n is the thermal conductivity

$$k_n = \left(\frac{5}{2} + c_n \right) \frac{k_B^2}{q} \cdot T_n \cdot \mu_n \cdot n \tag{14}$$

The DD mobility is modelled by

$$\mu_v^{LIF}(F_v) = \frac{\mu_v^{LIF}}{\left(1 + \left(\frac{\mu_v^{LI} \cdot F_v}{\upsilon_v^{sat}} \right)^{\beta_v} \right)^{1/\beta_v}}, \quad v = n, p \tag{15}$$

where F_v represents the driving force for electrons and holes, μ_v^{LI} is the zero-field mobility, and υ_v^{sat} is the saturation velocity

The HD mobility is modelled carrier temperature dependent

$$\mu_v^{LIT} = \frac{\mu_v^{LI}}{1 + \alpha_v \cdot (T_v - T_L)} \tag{16}$$

where

$$\alpha_v = \frac{3 \cdot k_B \cdot \mu_v^{LI}}{2 \cdot q \cdot \tau_\in \cdot (\upsilon_v^{sat})^2} \tag{17}$$

And $\tau_\in$ is the energy relaxation times, and υ_v^{sat} is the saturation velocity.

4 Results and discussion

The transfer characteristics and the small signal analysis have been studied.

Figure 6 I_D-V_G and G_m-V_G plots of GaN HEMT (gate length 250 nm) without FP using DD model (see online version for colours)

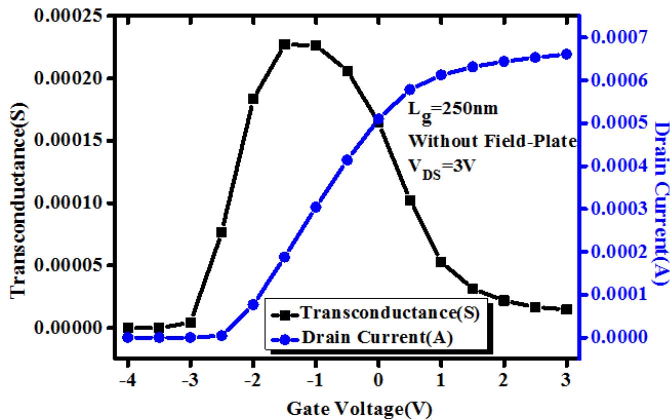

The DC transfer characteristics at V_{DS} = 3 V is shown in Figure 6. The I_D-V_G and transconductance (G_m) characteristics without FP length are shown.

Figure 7 I_D-V_D plot of GaN HEMT using DD model at V_{GS} = –2 to 2 V without FP (see online version for colours)

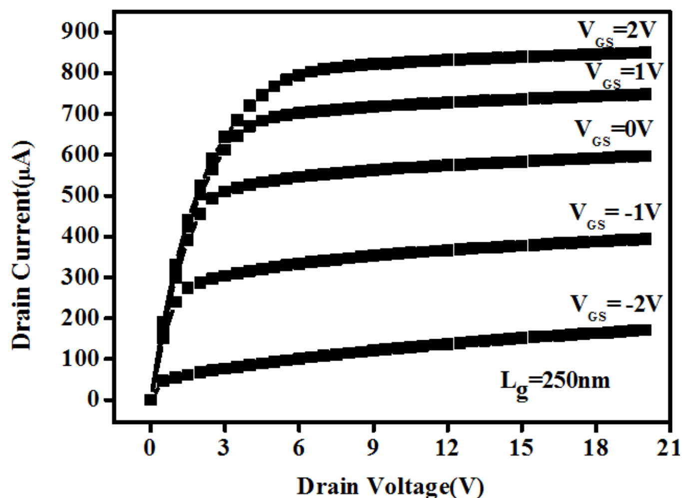

In Figure 7, the drain current increases linearly until it reaches the saturation region. The gate bias is swept from −2 to 2 V in a step of 1 V. The device exhibits maximum drain current (without FP) at V_{GS} = 2 V and the drain bias is swept from 0 to 20 V in a step of 5 V.

Figure 8 Electron concentration of GaN HEMT in the off-state (see online version for colours)

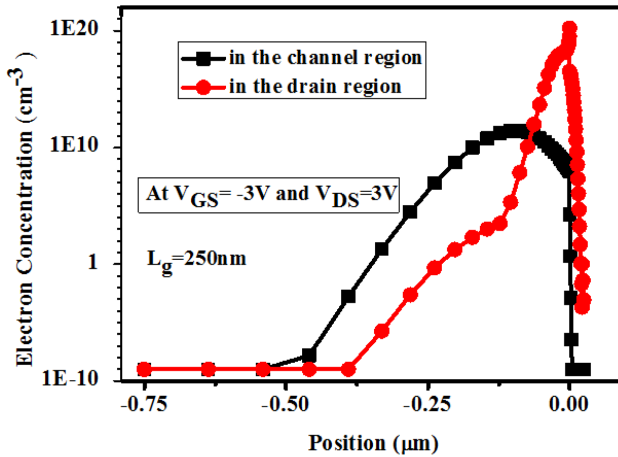

Notes: The red (filled circle) colour represents the electron concentration in the drain region and the black colour (filled square) represent the electron concentration in the channel region.

The electron concentration of the device in off-state shown in Figure 8. The electron concentration of the HEMT in the channel and drain region at V_{GS} = –3 V and V_{DS} = 3 V is shown in Figure 8. The cutline is taken from the channel and drain region.

Figure 9 Electron concentration of GaN HEMT in the on-state (see online version for colours)

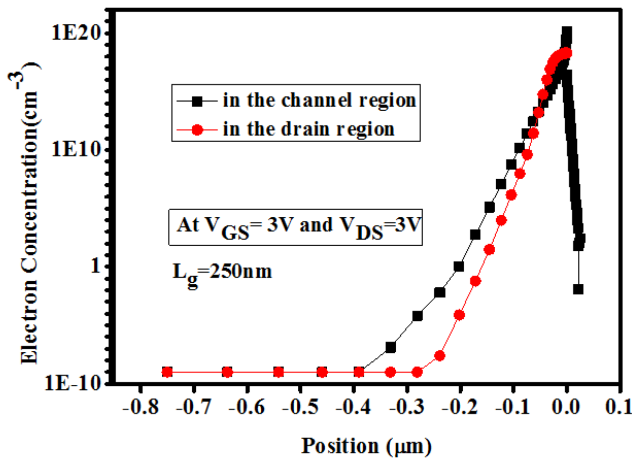

Notes: The red (filled circle) colour represents the electron concentration in the drain region and the black (filled square) colour represent the electron concentration in the channel region.

The electron concentration of the device in on-state shown in Figure 9. The electron concentration of the HEMT in the channel and drain region without FP at V_{GS} = 3 V and V_{DS} = 3 V is shown in Figure 9. The cutline is taken from the channel and the drain region. The most important is to estimate the effect of FP structure to the transfer characteristics, the device current gain, and cut-off frequency.

Figure 10 I_D-V_G plot of GaN HEMT at gate length 250nm with and without FP using DD and HD model at V_{DS} = 3 V (see online version for colours)

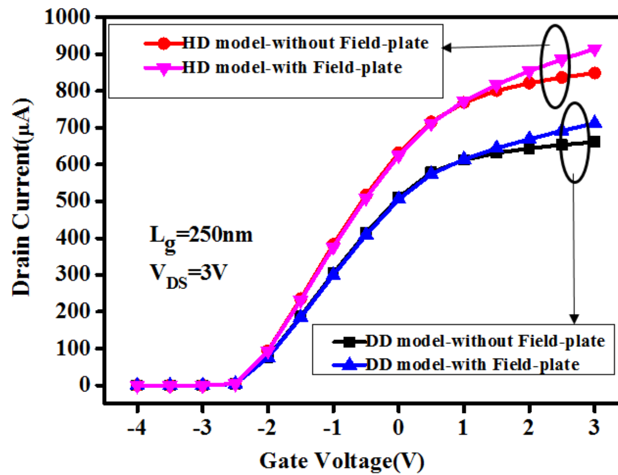

The measured transfer characteristics for V_{DS} = 3 V and L_g = 250 nm is shown in Figure 10 along with four simulated I_D-V_G plots i.e., DD model without and with FP and HD model without and with FP. Here the FP length is L_{FP} = 0.3 µm. The HD model simulated I_D-V_G plots show a significant increase in the drain current compared to the DD model without FP and with FP. With the increase in the gate voltage, the number of carrier concentration in the 2DEG is increased, and as a result of which the drain current increases. The drain current is linearly controlled by the gate voltage. There is a significant improvement in the I-V characteristics by applying the FP technique.

Figure 11 Current gain with and without FP at V_{DS} = 5 V (see online version for colours)

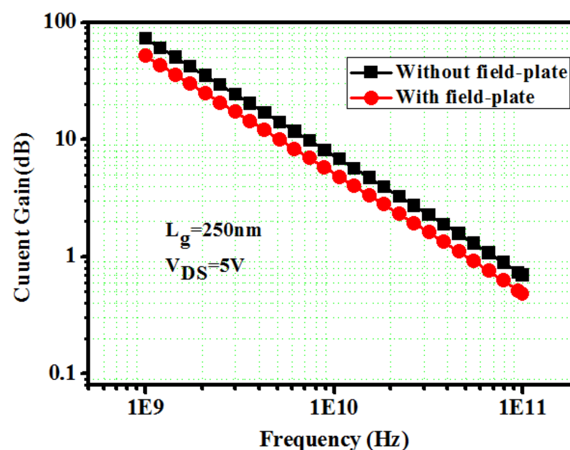

Notes: The red colour (filled circle) represents the current gain with the FP and the black colour (filled square) represents the current gain without a FP.

The RF performance of the device is evaluated by small signal AC analysis. The current gain $|h_{21}|$ for the 0.25 µm device is shown in Figure 11. The gain decreases at the higher

cut-off frequency. That is due to the gate capacitance which causes a frequency dependent gate current. The device with a FP has a larger gate area due to which the gate current increases.

The device gain decreases when the FP structure is added. The added parasitic capacitance between the FP and channel results in an increased device gate drain capacitance (C_{GD}). The increase in C_{GD} affects both current gain and the cut-off frequency in reducing these values. As the feedback capacitance C_{GD} increases and the extrinsic cut-off frequency i.e., f_t depends on C_{GD} in equation (18) without Miller effect correction. The corresponding f_t expression is given by

$$f_t = g_m / \left[2\pi \left(C_{GS} + C_{GD} \right) \right] \tag{18}$$

Figure 12 Cut-off frequency with and without FP at V_{DS} = 5 V (see online version for colours)

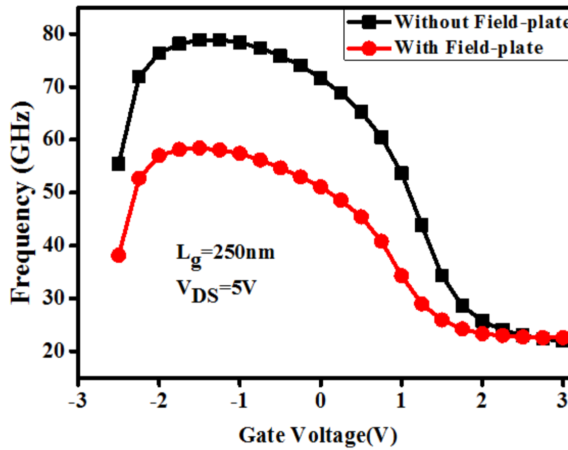

Notes: The red colour (filled circle) represents the cut-off frequency with the FP and the black colour (filled square) represents the cut-off frequency without a FP.

The cut-off frequency is lower for the transistor with the FP as shown in Figure 12. The slightly higher cut-off frequency for gate voltage above 1.5 V is due to the higher drain current compared to the one without the FP. The frequency characteristics are calculated without any interconnect structures or parasitic components of the measurement equipment. This causes a higher cut-off frequency than measured. The device current gain and cut-off frequency parameters for the added FP geometry have been extracted at a V_{GS} of –3 V to 3 V and at a V_{DS} of 5 V. The devices with FP show lower f_t values compared to that of the device without a FP. The formation of the gate capacitance between the FP terminal and the device channel leads to the addition of parasitic capacitance between gate and channel of the device due to which the device current gain cut-off frequency f_t decreases. The s-parameter data have been simulated to extract f_t.

5 Conclusions

This work has contributed to the overall understanding of AlGaN/GaN HEMTs, and a number of techniques developed for the design of high breakdown voltage HEMTs which

could potentially be beneficial in GaN technology. We study the electrostatics of the breakdown fields and the map the strain/stress profile as a function of FP length and height. We have presented the results on the performance of 0.25 μm gate length AlGaN/GaN HEMTs with and without FP. The gate connected FPs are very effective and by this technique, devices exhibited significant improvements. By adding FP geometry, the abasement in f_t values has been observed. Although present device operation is limited due to arise of excess capacitance from the FP. At higher frequencies, the operation can be attained by reducing gate length and/or optimising FP geometry with slant FPs (Pei et al., 2009). From the simulation results, it is shown that this technology has the ability to minimise both the DC and RF dispersion and parasitic capacitance. The present design has shown superior DC/RF device performance feasibility of GaN-based HEMTs for high power RF circuit applications. This study will help to give definitive direction in developing AlGaN/GaN HEMTs for power applications.

We demonstrate that TCAD can be advantageously used to map stress/strain at the nanoscale in an unexplored situation where the use of advanced diffraction pattern treatment is needed. We propose TCAD as an alternative for strain analysis in advanced devices like GaN-HEMTs.

References

Ambacher, O. et al. (2000) 'Two dimensional electron gases induced by spontaneous and piezoelectric polarization in undoped and doped AlGaN/GaN heterostructures', *Journal of Applied Physics*, Vol. 87, No. 1, pp.334–344.

Ando, Y. et al. (2003) '10-W/mm AlGaN-GaN HFET with a field modulating plate', *IEEE Electron Device Letters*, Vol. 24, No. 5, pp.289–291.

ATLAS Users Manual (*2017*).

Chiu, H. et al. (2013) 'Characteristics of AlGaN/GaN HEMTs with various field-plate and gate-to-drain extensions', *IEEE Transactions on Electron Devices*, Vol. 60, No. 11, pp.3877–3882.

Karmalkar, S. and Mishra, U.K. (2001) 'Enhancement of breakdown voltage in AlGaN/GaN high electron mobility transistors using a field plate', *IEEE Transactions on Electron Devices*, Vol. 48, No. 8, pp.1515–1521.

Minimos-NT User Manual (2017).

Mishra, U.K., Parikh, P. and Wu, Y.F., (2002) 'AlGaN/GaN HEMTs – an overview of device operation and applications', *Proceedings of the IEEE*, Vol. 90, No. 6, pp.1022–1031.

Pei, Y. et al. (2009) 'Deep-submicrometer AlGaN/GaN HEMTs with slant field plates', *IEEE Electron Device Letters*, Vol. 30, No. 4, pp.328–330.

Victory Device User Manual (2017).

Vitanov, S. et al. (2007) 'Predictive simulation of AlGaN/GaN HEMTs', *2007 IEEE Compound Semiconductor Integrated Circuits Symposium*, pp.1–4.

Vitanov, S. et al. (2012) 'Physics-based modeling of GaN HEMTs', *IEEE Transactions on Electron Devices*, Vol. 59, No. 3, pp.685–693.

Wu, Y. et al. (2008) 'A 97.8% efficient GaN HEMT boost converter with 300-W output power at 1 MHz', *IEEE Electron Device Letters*, Vol. 29, No. 8, pp.824–826.